

Supporting Information

Polyimide/ZIF-7 Mixed-Matrix Membranes: Understanding *in-situ* Confined Formation of ZIF-7 Phases inside Polymer and Their Effects on Gas Separations

Sunghwan Park,^{†a} Kie Yong Cho,^{†ab} and Hae-Kwon Jeong^{*ac}

^a Artie McFerrin Department of Chemical Engineering and ^c Department of Materials Science and Engineering, Texas A&M University, 3122 TAMU, College Station, TX 77843-3122, United States

^b Department of Industrial Chemistry, Pukyong National University, 45 Yongso-ro, Nam-gu, Busan 48513, Republic of Korea

† These authors contributed equally to this work.

* Corresponding author e-mail: hjeong7@tamu.edu (H.-K. Jeong)

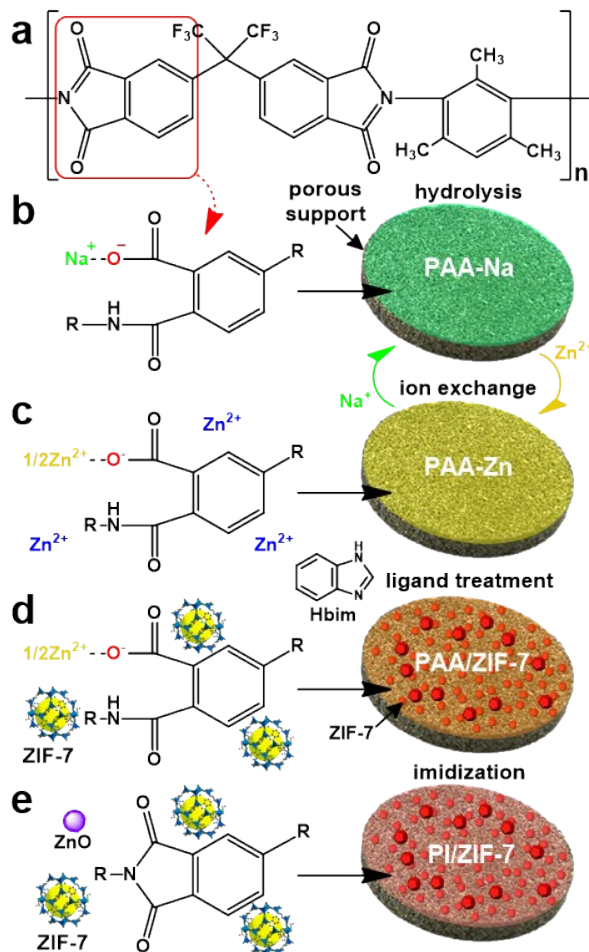


Fig. S1. Schematic of the PMMOF process using 6FDA-DAM: (a) pristine polyimide (PI), (b) poly(amic acid) sodium salt (PAA-Na), (c) poly(amic acid) zinc salt (PAA-Zn), (d) poly(amic acid) zinc salt with ZIF-7 (PAA/ZIF-7), and (e) polyimide with ZIF-7 (PI/ZIF-7).

PMMOF Process

The PMMOF process consists of the following steps:

Step 1) A PI was partially deimidized by a hydrolysis reaction using a sodium formate aqueous solution, resulting in a poly(amic acid) sodium salt (PAA-Na) (Fig. S1b).

Step 2) Sodium ions in the PAA-Na were exchanged with Zn ions, yielding a poly(amic acid) zinc salt (PAA-Zn) (Fig. S1c).

Step 3) ZIF-7 was formed inside the PAA-Zn matrix by solvothermally treating the sample in a bIm linker solution (PAA/ZIF-7) (Fig. S1d).

Step 4) PAA/ZIF-7 was imidized to form PI/ZIF-7 MMMs (Fig. S1e).¹

Polymer modifications characterizations

As shown in Fig. S2, the deimiziation step caused a decrease in the intensities of 1786 cm^{-1} and 1722 cm^{-1} peaks, which correspond to asymmetric and symmetric C=O stretching of imide groups in PI, respectively.^{2,3} Meanwhile, there was no change in the peak at 1485 cm^{-1} , which can be assigned to C-C stretching of benzene ring. The ratio of the intensities of the 1722 cm^{-1} and 1486 cm^{-1} peaks (i.e., $I_{\text{C=O}}/I_{\text{C-C}}$) was reduced from 5.2 ± 0.04 (PI) to 3.7 ± 0.2 (PAA-Na), indicating hydrolysis of imide group (Fig. S2).^{2,3} Furthermore, the uniform modification of PI films is important in order to acquire isotropic PI/ZIF-7 MMMs. To test the uniformity of modification, plasma etching was performed on a PAA-Na film to etch down to $\sim 1.7\text{ }\mu\text{m}$ thickness and then the corresponding chemical structure was examined using FT-IR. The peak intensity ratio between the symmetric C=O and C-C bands was well preserved in comparison to that of PAA-Na before etching, exhibiting $I_{\text{C=O}}/I_{\text{C-C}} = 3.3 \pm 0.3$ (Fig. S3). This supports the uniform deimidization throughout the PI film (Fig. S3).

Upon the ion exchange and the solvothermal ligand treatment, there was little peak intensity change in the FT-IR spectra relative to that of PAA-Na (Fig. S2). On the other hand, the peak position of the symmetric C=O was blue-shifted in PAA-Na (1722.4 cm^{-1}) and then largely red-shifted in PAA-Zn (1720 cm^{-1}) (Fig. S2). This observation is expected considering the fact that bond strength between coordinating metal ions and carboxylic groups in PAA depends on metal ions. Yu *et al.*⁴ also made similar observation which showed the red-shift of the carbonyl band in FT-IR by the coordination of cadmium and lead ions with the carboxylic group in poly(amic acid). Based on these FT-IR observations, it is reasoned that the metal ions possibly formed coordination bonds with the carboxylic groups in PAA, not merely absorbed into the free volume of the film. In the fourth step, the imidization of PAA led to an increase in the intensity of the C=O peaks as much as that of the pristine polymer ($I_{\text{C=O}}/I_{\text{C-C}} = 4.8 \pm 0.2$) (Fig. S2). The slightly lower C=O peak intensity compared with that of the pristine PI can be explained by the fact that some of Zn ions coordinated with PAA likely remained because of their multiple coordination bonds, thereby leading to incomplete imidization.⁵ Our plausible description regarding imidization of PAA can be supported by the almost restoration of the C=O peak position (1722 cm^{-1}) in comparison to that of PAA-Zn (Fig.S2).

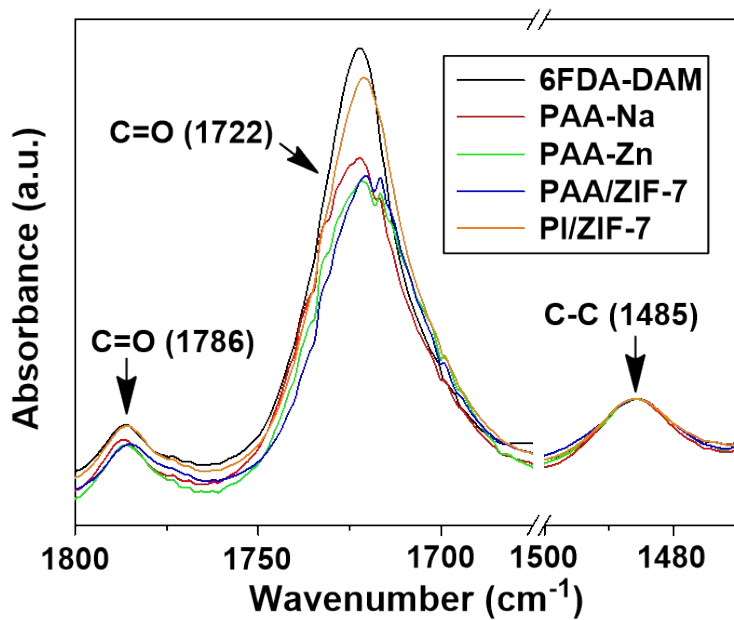


Fig. S2. Evolution of FT-IR spectra of samples at each stage during PMMOF in comparion with 6FDA-DAM polyimide.

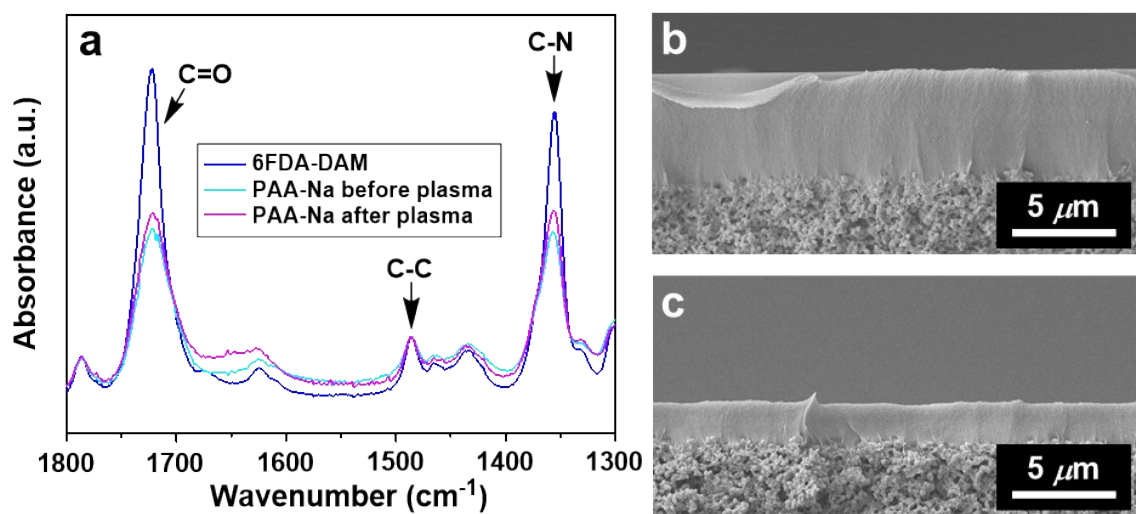


Fig. S3. (a) FT-IR spectra of 6FDA-DAM and before/after oxygen plasma etching of PAA-Na. Cross-sectional SEM images of (b) before and (c) after oxygen plasma etching of PAA-Na (oxygen plasma etching was performed for 1 h).

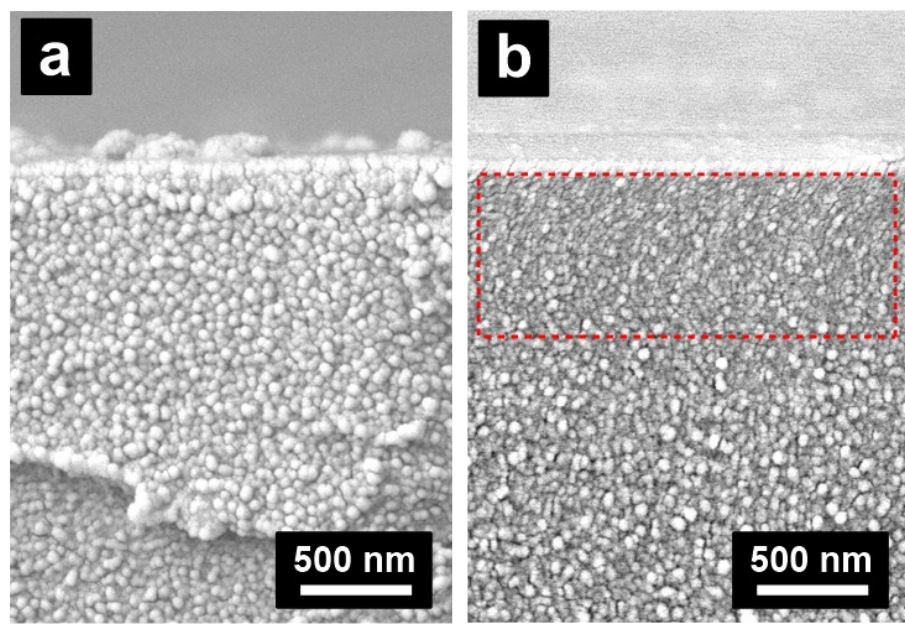


Fig. S4. Cross-sectional SEM images of PI/ZIF-7-I before (a) and after acid treatment (b).

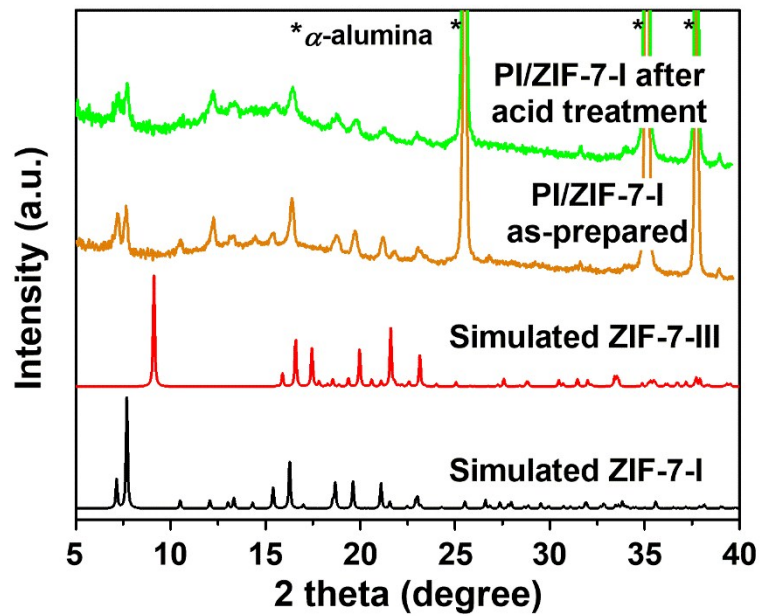


Fig. S5. XRD patterns of PI/ZIF-7-I before and after acid treatment.

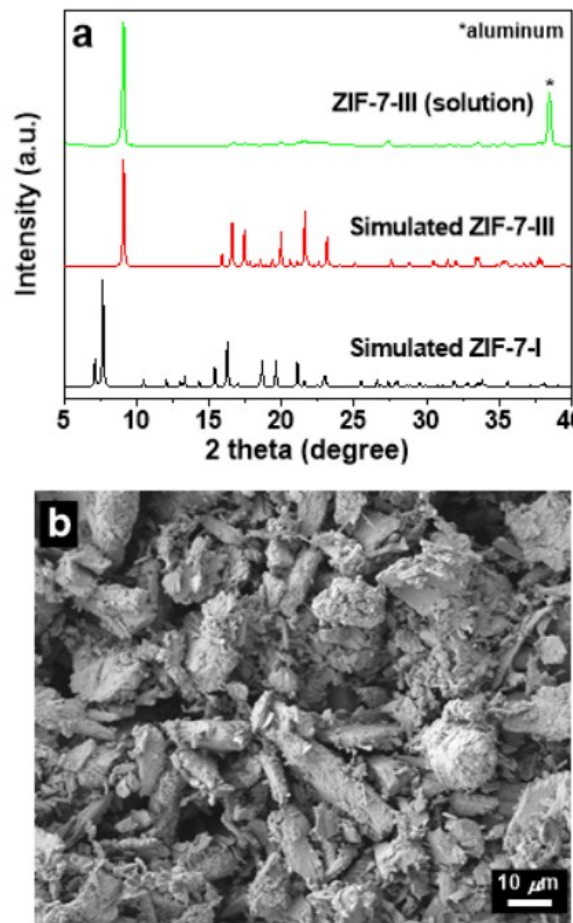


Fig. S6. (a) XRD patterns of ZIF-7-III synthesized in a bulk solution (i.e., ZIF-7-III (solution)). (b) SEM image of ZIF-7-III (solution).

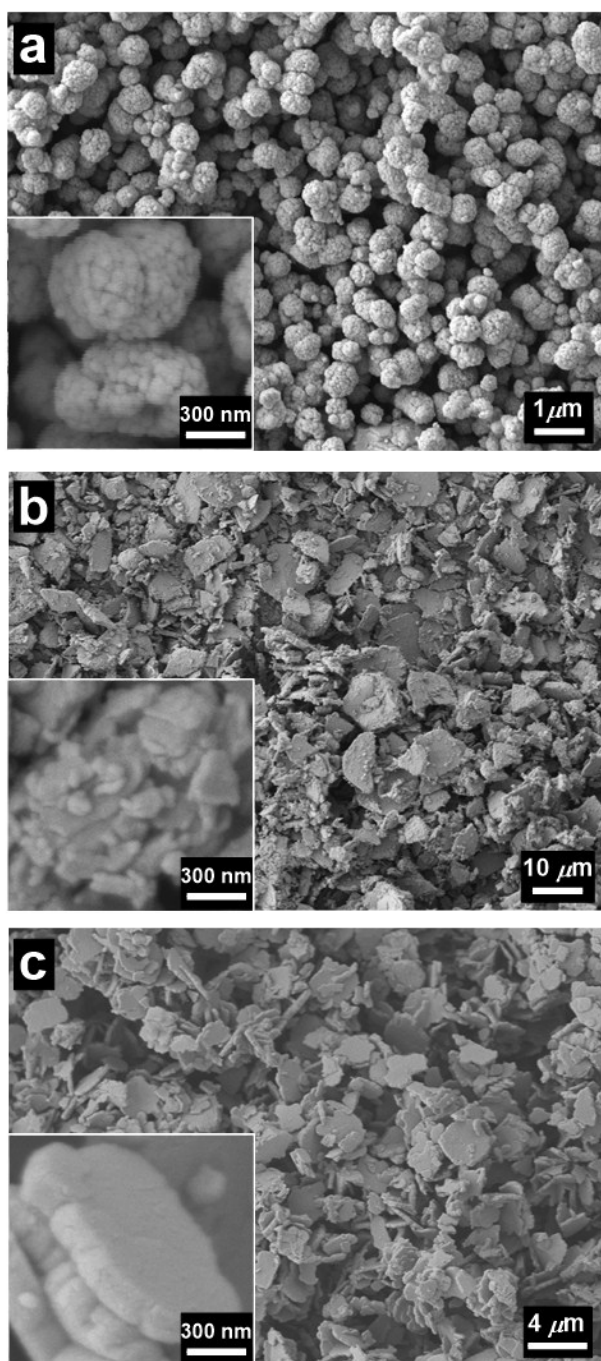


Fig. S7. SEM images of ZIF-7 particles prepared using solution reaction. Zinc and bim molarity of each crystal phase is as follows; (a) 0.042 mol kg⁻¹ of zinc and 1.054 mol kg⁻¹ of bim for ZIF-7-I, (b) 0.083 mol kg⁻¹ of zinc and 1.054 mol kg⁻¹ of bim for ZIF-7-mix, and (c) 0.105 mol kg⁻¹ of zinc and 1.054 mol kg⁻¹ of bim for ZIF-7-III (the inset images exhibited surface of particles).

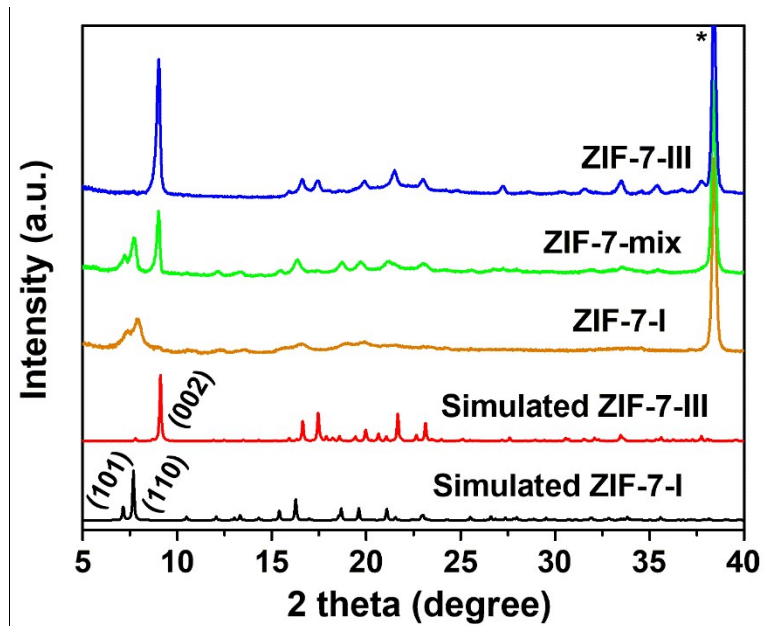


Fig. S8. XRD patterns of ZIF-7 particles.

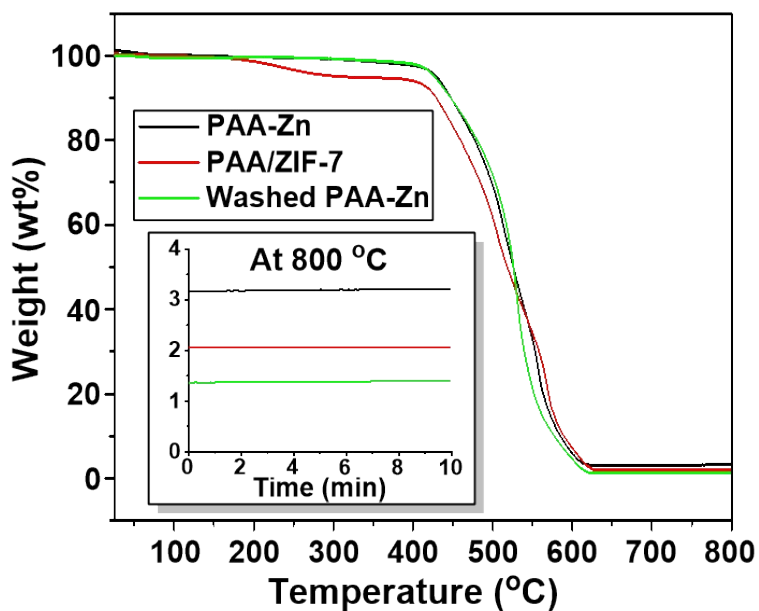


Fig. S9. TGA thermogram of polymers containing zinc.

Residue weights were used to calculate the concentration of mobile zinc ions. It should be noted that the zinc ions in PAA-Zn consist of mobile ions as well as immobile ions coordinated to the polymer (Fig. S8b).^{6,7} Upon thoroughly washing, most of mobile ions were removed while immobile zinc ions still remaining in washed PAA-Zn (Fig. S8c).^{6,7} Thus, the weight of mobile zinc ions was determined by subtracting the weight of zinc coordinated with the polymer based on washed PAA-Zn from the zinc weight of PAA-Zn. Also, the weight of zinc ions in PAA/ZIF-7 was determined by the same manner.

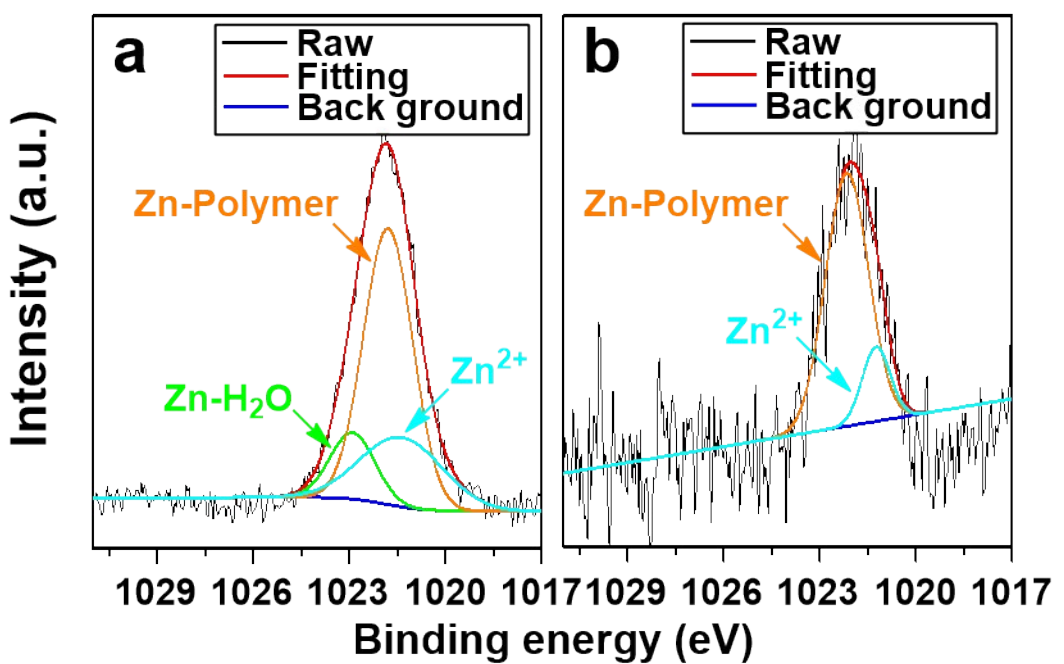


Fig. S10. XPS spectra of PAA-Zn without washing (a) and with washing (b).

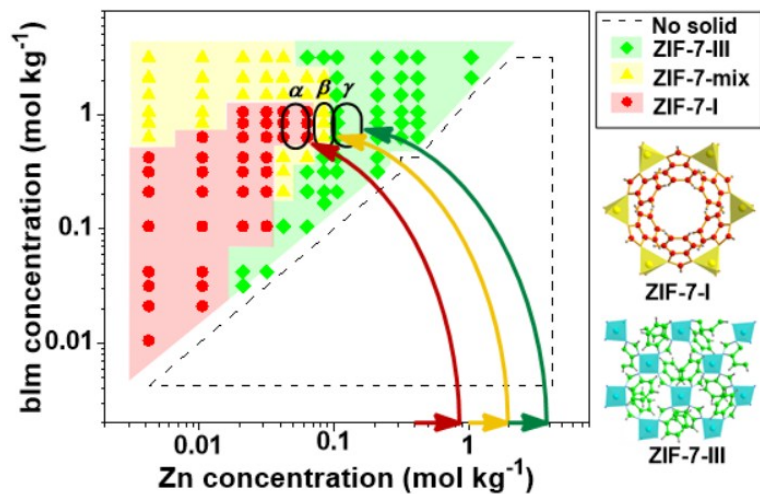


Fig. S11. ZIF-7 crystal phase diagram and the traced PMMOF reaction conditions at different zinc concentrations in ion exchange solutions.

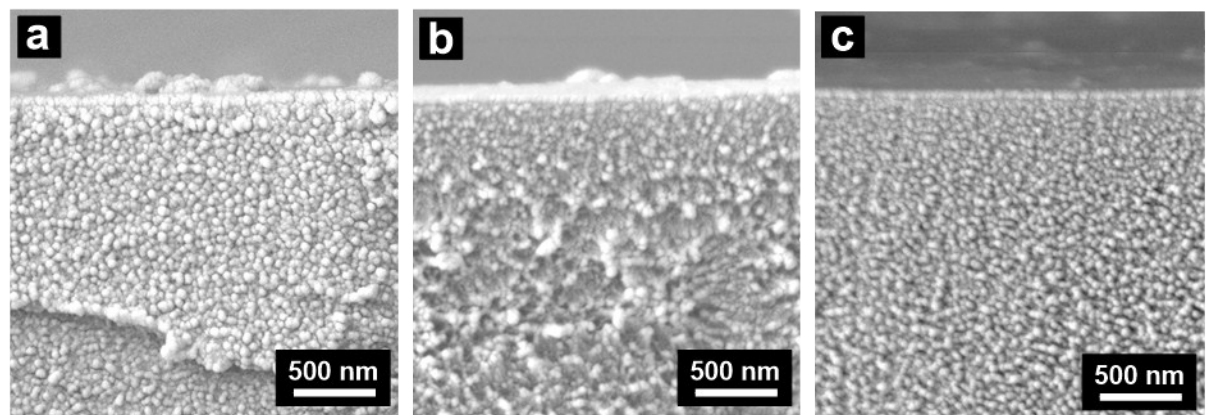


Fig. S12. SEM images of PI/ZIF-7 MMMs with different crystal phases: (a) PI/ZIF-7-I, (b) PI/ZIF-7-mix, and (c) PI/ZIF-7-III.

Table S1. Weight percentages of ZnO induced by thermal oxidization and that of calculated ZIF-7 in a polymer.

Sample	Total ZnO wt%	ZIF-7 derived ZnO wt%	ZIF-7-I wt%	ZIF-7-III wt%	Total ZIF-7 wt%
Washed PAA-Zn	1.38	0.00	0.00	0.00	0.00
ZIF-7-I	25.5	25.5	100	0.00	100
ZIF-7-III	26.3	26.3	0.00	100	100
PI/ZIF-7-I	2.09	0.71	2.78	0.00	2.78
PI/ZIF-7-mix	3.19	1.81	3.63	3.37	7.00
PI/ZIF-7-III	4.00	2.62	0.00	9.96	9.96

Determination of ZIF-7 loadings based TGA

The loading percentages of ZIF-7 in polymer were obtained by the contents of residue of thermal oxidation using Equation S1 as follows:

$$ZIF-7 \text{ wt\% in PI/ZIF-7} = \frac{W_{ZnO \text{ from PI/ZIF-7}} - W_{ZnO \text{ from PAA - Zn}}}{W_{ZnO \text{ from pure ZIF-7}}} \times 100(\%) \quad (S1).$$

Where W is a residual weight percentage of thermal decomposition. It is supposed that, upon thermal oxidation up to 800 °C, the MMMs and ZIF-7 were completely transformed to ZnO. For MMMs, there are two possible zinc sources forming ZnO: 1) zinc derived from *in-situ* grown ZIF-7 in polymer and 2) zinc coordinated to polymer. To avoid overestimation of ZIF loading, the content of zinc coordinated to polymer was determined by thermally oxidizing PAA-Zn and the resulting ZnO percentages (i.e., ~1.4 wt%) were subtracted from the total ZnO percentages of MMMs. The ZIF-7 loading percentages in MMMs were calculated based on the weight percentages of ZnO in MMMs and that of ZnO in each ZIF-7 phase.

For PI/ZIF-7-mix, it was assumed that the ZnO wt% of each ZIF-7 crystal phase is proportional to the percentage of corresponding ZIF-7 crystal phase. In this regard, ZIF-7-I wt% of PI/ZIF-7-mix was roughly estimated using the following equation:

$$\begin{aligned}
& ZIF-7-I \text{ wt\% in PI/ZIF-7-mix} \\
& = \left(\frac{A_{(101)} + A_{(110)}}{A_{(101)} + A_{(110)} + A_{(002)}} \right) \times \left(\frac{W_{ZnO \text{ from PI/ZIF-7-mix}} - W_{ZnO \text{ from PAA-Zn}}}{W_{ZnO \text{ from pure ZIF-7-I}}} \right) \\
& \times 100(\%) \quad (S2).
\end{aligned}$$

Where A is an integration area of each crystal plane determined by XRD patterns.

Table S2. Summary of single gas permeation results at 1 atm and room temperature.

Sample	Permeability (Barrer)				Selectivity				
	H ₂	CO ₂	N ₂	CH ₄	H ₂ /CO ₂	H ₂ /N ₂	H ₂ /CH ₄	CO ₂ /N ₂	CO ₂ /CH ₄
6FDA-DAM	589.17 ± 59.05	433.63 ± 105.38	19.24 ± 4.81	14.65 ± 1.18	1.36 ± 0.19	30.62 ± 4.59	40.23 ± 0.80	22.54 ± 0.16	29.61 ± 4.82
PI/ZIF-7-I	921.44 ± 100.46	407.41 ± 50.05	25.51 ± 1.57	13.67 ± 1.20	2.26 ± 0.03	36.12 ± 1.72	67.42 ± 1.45	15.97 ± 0.98	29.81 ± 1.05
PI/ZIF-7-mix	478.27 ± 44.76	116.83 ± 28.09	15.08 ± 3.06	5.59 ± 0.52	4.09 ± 0.60	31.71 ± 3.46	85.54 ± 0.01	7.75 ± 0.29	20.90 ± 3.06
PI/ZIF-7-III	322.01 ± 28.66	74.08 ± 1.73	5.42 ± 1.24	1.87 ± 0.07	4.35 ± 0.29	59.45 ± 8.27	172.24 ± 8.50	13.68 ± 2.80	39.63 ± 0.65

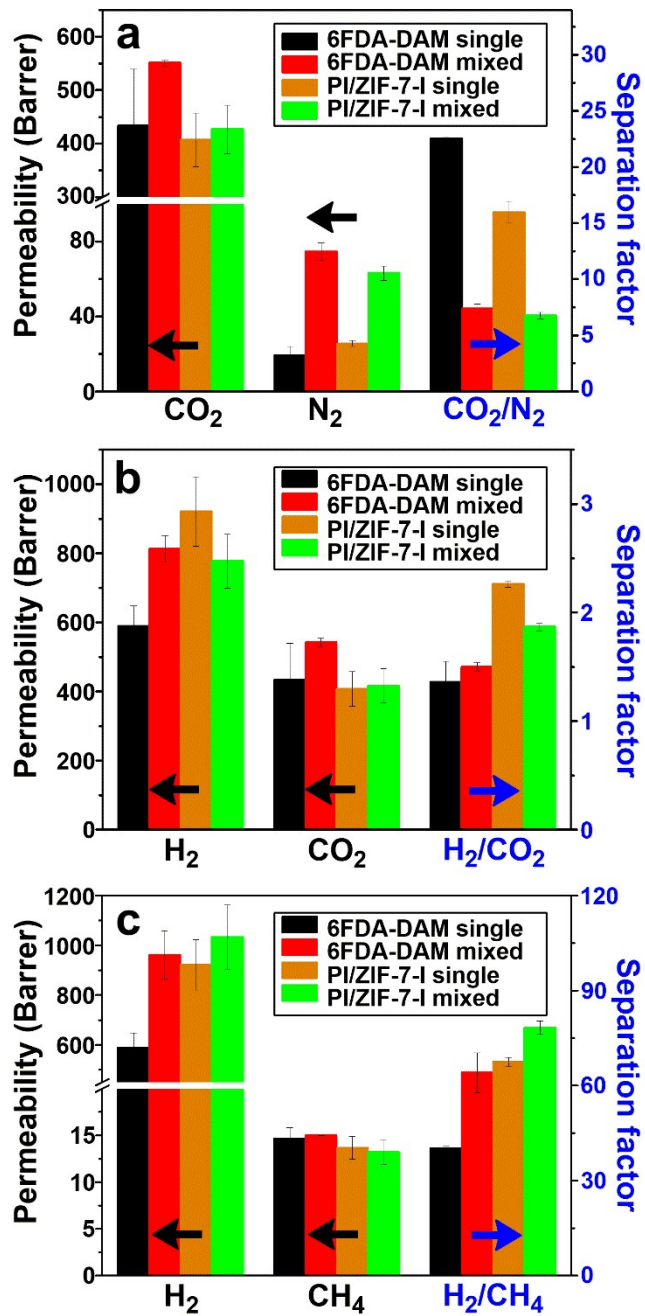


Fig. S13. Mixed gas separation results of 6FDA-DAM and PI/ZIF-7-I for binary gas mixtures of (a) CO₂/N₂, (b) H₂/CO₂, and (c) H₂/CH₄.

Mixed gas separation results

For mixed gas separations, three representative gas pairs (CO₂/N₂, H₂/CO₂, and H₂/CH₄) were tested for 6FDA-DAM and PI/ZIF-7-I MMMs. As compared with the single gas separation, the mixed gas separation factors were depressed except for H₂/CH₄ likely due to the competition

between two different gas molecules (Fig. S12).⁸ In particular, the substantial decrease in CO₂/N₂ separation factor (~ 60 %) was observed as shown in Fig. S12a. For H₂/CO₂ binary gas mixture, 6FDA-DAM showed relatively higher H₂ permeability than that for single gas (Fig. S12b). Meanwhile, the PI/ZIF-7-I MMMs exhibited lower H₂ permeability in binary gas permeation than in single gas permeation (Fig. S12b). As such, the H₂/CO₂ separation factor of 6FDA-DAM showed slightly lower in binary gas (Fig. S12b). In contrast, the PI/ZIF-7-I MMMs showed lower separation factor in binary gas (Fig. S12b), possibly resulting from stronger sorption competition between H₂ and CO₂ in PI/ZIF-7-I than that in 6FDA-DAM.⁹ Similarly, although both 6FDA-DAM and PI/ZIF-7-I showed an increase in the binary H₂/CH₄ separation factor, 6FDA-DAM exhibited a larger increment than that shown by PI/ZIF-7 (Fig. S12c).

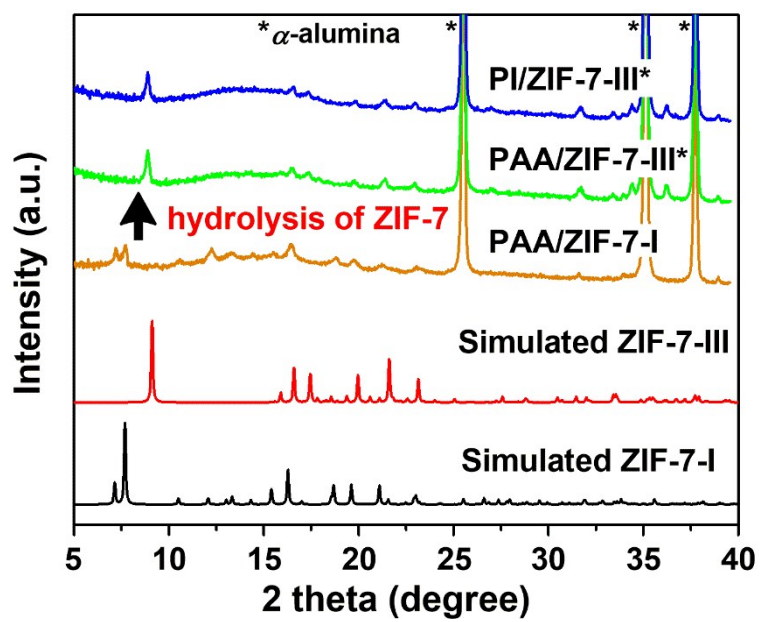


Fig S14. XRD patterns of PAA/ZIF-7-I, PAA/ZIF-7-III*, and PI/ZIF-7-III*.

Table S3. H₂/CO₂ separation performances of the reported MMMs.

Polymer	Filler	Wt% of filler	H ₂ permeability	H ₂ /CO ₂ selectivity	Ref.
Matrimid®5218	C-MOF-5	30	53.8 (120.5 %)	2.66 (-1.8 %)	10
PES	SAPO-34	20	12.57 (82.2 %)	2.45 (2.1 %)	11
Matrimid®5218	hollow silicalite-1	8	38.4 (26.3 %)	2.1 (46.2 %)	12
PBI	ZIF-7	50	26.2 (608.1 %)	14.9 (71.3 %)	13
Matrimid®9725	Zeolite 4A	30	101.60 (464 %)	2.10 (-16 %)	14
6FDA:DSDA/4MPD:4,4'-SDA	NH2-MIL-101	10	114 (26.7 %)	1.6 (3.3 %)	15
6FDA-durene	ZIF-8	15	2136.6 (312.1 %)	1.4 (27.3 %)	16
X-linked 6FDA-durene	ZIF-8	33.3	283.5 (444.1 %)	12.0 (-90.8 %)	
PEI	C-MOF-5	25	28.32 (181.2 %)	5.25 (-12.4 %)	17
PPO	Silica	10	548.7 (567.8 %)	3.6 (111.9 %)	18
Matrimid®5218	MIL-53-ht	37.5	103.0 (300.8 %)	2.02 (-34.2 %)	19
Matrimid®5218	MIL-53-as	37.5	66.0 (156.8 %)	1.68 (-45.3 %)	
VTEC™	NH2-MIL-53	20	5.1 (13.3 %)	7.0 (16.7 %)	20
6FDA-DAM	ZIF-11	20	272.45 (1173.1 %)	1.06 (2.9 %)	2
PI	MWCNT@GONRs	2	42.5 (42 %)	1.7 (-15 %)	21
Matrimid®5218	ZIF-11	40	28.36 (63.6 %)	2.84 (-31.2 %)	22
CA	C-MOF-5	12	14.95 (247.7 %)	1.78 (61.8 %)	23
CA	T-MOF-5	12	13.90 (223.3 %)	1.79 (62.7 %)	
6FDA-TTM	Si-H	10	76.5 (86.1 %)	2.1 (40.0 %)	24
P84	Nanodiamond	1	6.7 (-16.3 %)	4.1 (13.8 %)	25
PAI	MOF-1	30	191 (141.2 %)	1.8 (5.9 %)	26
PSf	HKUST-1	10	15.0 (53.1 %)	1.9 (18.8 %)	27
PSf	Mn(HCOO)2	10	10.5 (7.1 %)	1.6 (0.0 %)	
Matrimids5218	Cu-BPY-HFS	30	20.3 (16.0 %)	2.0 (-16.7 %)	28
Matrimids5218	MOF-5	20	114.9 (247.1 %)	3.0 (-9.1 %)	29
Ultem1000	MOF-5	20	16.9	5.7	

			(50.9 %)	(0.0 %)	
Matrimids5218	HKUST-1	30	66.9 (102.1 %)	3.0 (-9.1 %)	
Matrimids	MOF-5	30	53.8 (120.5 %)	2.7 (0.0 %)	30
Matrimids	ZIF-8	60	35.8 (23.9 %)	4.4 (41.9 %)	31
PPEEs	ZIF-8	30	92.3 (1068 %)	1.8 (28.6 %)	32
Matrimids	ZIF-8	30	112.1 (242.8 %)	3.9 (-2.5 %)	33
PBI	ZIF-8	30	105.4 (2749 %)	12.3 (43.0 %)	34
PBI	ZIF-8	30	82.5 (1912 %)	12.0 (34.8 %)	35
PIM-1	ZIF-8	43	6680 (309.8 %)	1.1 (450.0 %)	36
PBI	ZIF-90	45	24.5 (497.6 %)	25 (180.9 %)	37
PPO	HKUST-1	40	119 (58.7 %)	1.0 (-9.1 %)	38
6FDA:DSDA-4MPD:4,4'-SDA (1:1)	NH2-MIL-53(Al)	15	100 (11.0 %)	1.8 (12.5 %)	39
	NH2-MIL-101(Al)	10	114 (26.5 %)	1.6 (0.0 %)	
6FDA-4MPD:4,4'-SDA (1:1)	NH2-MIL-53(Al)	10	175 (3.6 %)	1.3 (0.0 %)	
	NH2-MIL-101(Al)	10	191 (13.0 %)	1.3 (0.0 %)	
PMMA	NH2-CAU-1	15	11 000 (120.0 %)	13 (333.3 %)	40
PSf	Silica-ZIF-8 core–shell	32	224.1 (540.3 %)	3.9 (14.7 %)	41
PBI-Bul	ZIF-8	30	22.1 (256.5 %)	4.2 (55.6 %)	42
DMPBIBul	ZIF-8	30	127.5 (896.1 %)	2.4 (-29.4 %)	
DBzPBI-Bul	ZIF-8	20	180.3 (193.6 %)	2.0 (-16.7 %)	
PBI	ZIF-11	39.5	464.7 (2602 %)	3.6 (-28.0 %)	43
Matrimid®5218	Silicalite	10	34.0 (12.2 %)	3.2 (0.0 %)	44
	SAPO-34	10	40.2 (32.7 %)	3.2 (0.0 %)	
	ZIF-8	10	51.1 (68.6 %)	3.0 (-6.3 %)	
Matrimid®5218	ZIF-11	25	95.9 (335.9 %)	4.4 (41.9 %)	45
		10	535 (52.9 %)	9.1 (13.8 %)	
PBI	Cu ₂ (ndc) ₂ (dabco)	20	6.13 (152.0 %)	26.7 (181.1 %)	46
6FDA-DAM	ZIF-7-I	2.78	921.44	2.26	This

		(56.4 %)	(66.2 %)	work
ZIF-7-mix	7.00	478.27 (-18.8 %)	4.09 (200.7 %)	
ZIF-7-III	9.96	322.01 (-45.4 %)	4.35 (219.9 %)	
ZIF-7-III*	2.78	1630.44 (176.7 %)	3.82 (180.9 %)	

Note: the unit of permeability is Barrer (i.e., 1 Barrer = 10^{-10} cm³(STP) cm cm⁻² cmHg⁻¹ sec⁻¹).
The percentages in the round bracket of H₂ permeability and H₂/CO₂ selectivity indicate the changing percentages of MMMs from its corresponding polymer.

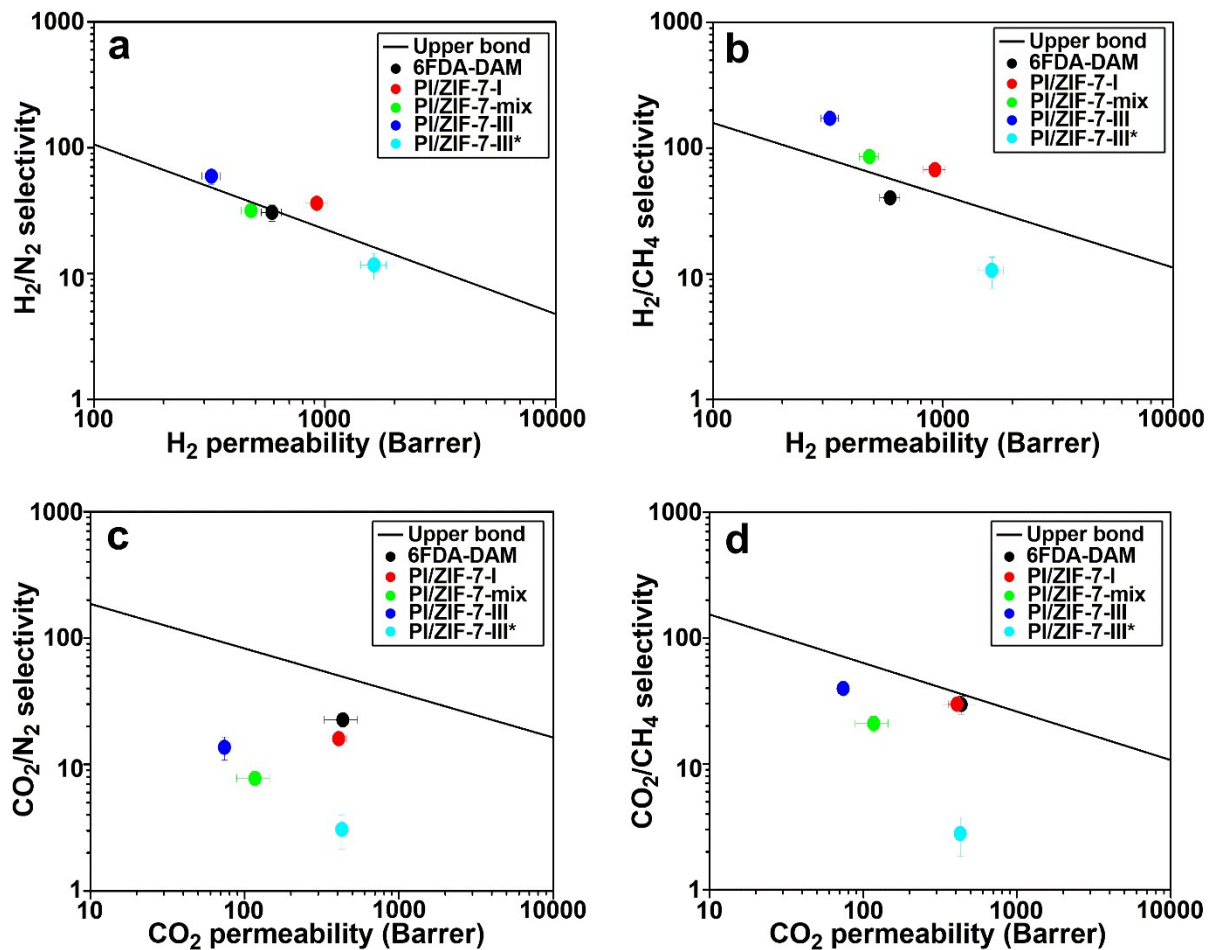


Fig. S15. Upper bound plot of 6FDA-DAM and PI/ZIF-7 MMMs. (a) H_2/N_2 separation, (b) H_2/CH_4 separation, (c) CO_2/N_2 separation, and (d) CO_2/CH_4 separation.⁴⁷

Reference

1. S. Park, M. R. Abdul Hamid and H.-K. Jeong, *Acs Appl Mater Inter*, 2019, **11**, 25949-25957.
2. M. S. Boroglu and A. B. Yumru, *Sep Purif Technol*, 2017, **173**, 269-279.
3. Y. Xu, A. L. Zhao, X. L. Wang, H. Xue and F. L. Liu, *J Wuhan Univ Technol*, 2016, **31**, 1137-1143.
4. J. X. Yu, M. Tong, X. M. Sun and B. H. Li, *Biochem Eng J*, 2007, **33**, 126-133.
5. W. G. Dong, G. H. Kim, J. Y. Choi, J. R. Ybon and Y. H. Kim, *Colloid Surface A*, 2008, **324**, 122-125.
6. S. Park, M. R. A. Hamid and H. K. Jeong, *Acs Appl Mater Inter*, 2019, **11**, 25949-25957.
7. M. R. A. Hamid, S. Park, J. S. Kim, Y. M. Lee and H. K. Jeong, *J Mater Chem A*, 2019, **7**, 9680-9689.
8. S. Park, A. S. Lee, Y. S. Do, J. F. Kim, S. S. Hwang, Y. M. Lee, J. H. Lee and J. S. Lee, *Journal of Membrane Science*, 2016, **516**, 202-214.
9. J. E. Bachman and J. R. Long, *Energ Environ Sci*, 2016, **9**, 2031-2036.
10. E. V. Perez, K. J. Balkus, J. P. Ferraris and I. H. Musselman, *Journal of Membrane Science*, 2009, **328**, 165-173.
11. E. Karatay, H. Kalipcilar and L. Yilmaz, *Journal of Membrane Science*, 2010, **364**, 75-81.
12. B. Zornoza, O. Esekhile, W. J. Koros, C. Tellez and J. Coronas, *Sep Purif Technol*, 2011, **77**, 137-145.
13. T. X. Yang, Y. C. Xiao and T. S. Chung, *Energ Environ Sci*, 2011, **4**, 4171-4180.
14. J. Ahmad and M. B. Hagg, *Sep Purif Technol*, 2013, **115**, 190-197.
15. B. Seoane, C. Tellez, J. Coronas and C. Staudt, *Sep Purif Technol*, 2013, **111**, 72-81.
16. S. N. Wijenayake, N. P. Panapitiya, S. H. Versteeg, C. N. Nguyen, S. Goel, K. J. Balkus, I. H. Musselman and J. P. Ferraris, *Ind Eng Chem Res*, 2013, **52**, 6991-7001.
17. M. Arjmandi and M. Pakizeh, *J Ind Eng Chem*, 2014, **20**, 3857-3868.
18. G. L. Zhuang, H. H. Tseng and M. Y. Wey, *Int J Hydrogen Energ*, 2014, **39**, 17178-17190.
19. J. O. Hsieh, K. J. Balkus, J. P. Ferraris and I. H. Musselman, *Micropor Mesopor Mat*, 2014, **196**, 165-174.
20. E. V. Perez, G. J. D. Kalaw, J. P. Ferraris, K. J. Balkus and I. H. Musselman, *Journal of Membrane Science*, 2017, **530**, 201-212.
21. Q. Z. Xue, X. L. Pan, X. F. Li, J. Q. Zhang and Q. K. Guo, *Nanotechnology*, 2017, **28**.
22. A. B. Yumru, M. Safak Boroglu and I. Boz, 2018, **8**, 529-541.
23. M. Arjmandi, M. Pakizeh, M. Saghi and A. J. P. C. Arjmandi, 2018, **58**, 317-329.
24. M. Lanč, P. Sysel, M. Šoltys, F. Štěpánek, K. Fónod, M. Klepić, O. Vopička, M. Lhotka, P. Ulbrich and K. Friess, *Polymer*, 2018, **144**, 33-42.
25. A. Pulyalina, G. Polotskaya, V. Rostovtseva, Z. Pientka and A. Toikka, *Polymers-Basel*, 2018, **10**.
26. *United States Pat*, US7658784B2, 2010.
27. A. Car, C. Stropnik and K.-V. Peinemann, *Desalination*, 2006, **200**, 424-426.
28. Y. Zhang, I. H. Musselman, J. P. Ferraris and K. J. Balkus, *J Membrane Sci*, 2008, **313**, 170-181.

29. *United States Pat.*, US7637983B1, 2009.
30. E. V. Perez, K. J. Balkus, J. P. Ferraris and I. H. Musselman, *J Membrane Sci*, 2009, **328**, 165-173.
31. M. J. C. Ordoñez, K. J. Balkus, J. P. Ferraris and I. H. Musselman, *J Membrane Sci*, 2010, **361**, 28-37.
32. K. Díaz, M. López-González, L. F. del Castillo and E. Riande, *J Membrane Sci*, 2011, **383**, 206-213.
33. Q. Song, S. K. Nataraj, M. V. Roussenova, J. C. Tan, D. J. Hughes, W. Li, P. Bourgoin, M. A. Alam, A. K. Cheetham, S. A. Al-Muhtaseb and E. Sivaniah, *Energy & Environmental Science*, 2012, **5**, 8359-8369.
34. T. Yang, G. M. Shi and T.-S. Chung, 2012, **2**, 1358-1367.
35. T. Yang and T.-S. Chung, *International Journal of Hydrogen Energy*, 2013, **38**, 229-239.
36. A. F. Bushell, M. P. Attfield, C. R. Mason, P. M. Budd, Y. Yampolskii, L. Starannikova, A. Rebrov, F. Bazzarelli, P. Bernardo, J. Carolus Jansen, M. Lanč, K. Friess, V. Shantarovich, V. Gustov and V. Isaeva, *J Membrane Sci*, 2013, **427**, 48-62.
37. T. Yang and T.-S. Chung, *J Mater Chem A*, 2013, **1**, 6081-6090.
38. L. Ge, W. Zhou, V. Rudolph and Z. Zhu, *J Mater Chem A*, 2013, **1**, 6350-6358.
39. B. Seoane, V. Sebastián, C. Téllez and J. Coronas, *CrystEngComm*, 2013, **15**, 9483-9490.
40. L. Cao, K. Tao, A. Huang, C. Kong and L. Chen, *Chem Commun*, 2013, **49**, 8513-8515.
41. S. Sorribas, B. Zornoza, C. Téllez and J. Coronas, *J Membrane Sci*, 2014, **452**, 184-192.
42. A. Bhaskar, R. Banerjee and U. Kharul, *J Mater Chem A*, 2014, **2**, 12962-12967.
43. L. Li, J. Yao, X. Wang, Y.-B. Cheng and H. Wang, 2014, **131**.
44. D. Carter, F. H. Tezel, B. Kruczak and H. Kalipcilar, *J Membrane Sci*, 2017, **544**, 35-46.
45. J. Sánchez-Laínez, B. Zornoza, Á. Mayoral, Á. Berenguer-Murcia, D. Cazorla-Amorós, C. Téllez and J. Coronas, *J Mater Chem A*, 2015, **3**, 6549-6556.
46. Z. Kang, Y. Peng, Z. Hu, Y. Qian, C. Chi, L. Y. Yeo, L. Tee and D. Zhao, *J Mater Chem A*, 2015, **3**, 20801-20810.
47. L. M. Robeson, *J Membrane Sci*, 2008, **320**, 390-400.